ARMA 22–674

Effect of casing stand-off on cracks creation around the wellbore

Agofack, N.
SINTEF Industry, Petroleum department, Trondheim, Norway
Larsen, I.; Opedal, N.; Skorpa, R.
SINTEF Industry, Petroleum department, Trondheim, Norway

Copyright 2021 ARMA, American Rock Mechanics Association
This paper was prepared for presentation at the 55th US Rock Mechanics/Geomechanics Symposium held in Houston, Texas, USA, 20-23 June 2021. This paper was selected for presentation at the symposium by an ARMA Technical Program Committee based on a technical and critical review of the paper by a minimum of two technical reviewers. The material, as presented, does not necessarily reflect any position of ARMA, its officers, or members. Electronic reproduction, distribution, or storage of any part of this paper for commercial purposes without the written consent of ARMA is prohibited. Permission to reproduce in print is restricted to an abstract of not more than 200 words; illustrations may not be copied. The abstract must contain conspicuous acknowledgement of where and by whom the paper was presented.

ABSTRACT: Cement sheath plays important role for the integrity of injection/production wells in subsurface activities. During the life of the well, mechanical and thermal loadings are applied to the casing and can lead to cracking the cement sheath and thus the loss of integrity. Additionally, the placement of the cement can also lead to the casing stand-off. To analyze these effects a modified discrete element method (MDEM) is used. Realistic cement and formation properties are used. Isotropic and anisotropic boundary stresses are investigated. The casing pressures considered are relevant for field operations such as during a casing test, XLOT (extended leak-off test) and hydraulic fracturing. The simulation results, show that in addition to the casing stand-off, several other parameters such as the casing pressure, the boundary stress, the cement, and rock properties, affect the cracks behind the casing. It was also observed that the casing stand-off become important in affecting the crack creation when it is around 0%. For values more 50%, no major difference was observed when compared to a centralized casing (100% stand-off).

1. INTRODUCTION

In many subsurface activities including hydrocarbon exploitation, carbon dioxide (CO_2) or hydrogen storage, the injection/production wells play important role. These wells are made by drilling a hole in the ground, running a steel tubular (called *casing*) into that hole, and pumping a cement slurry to fill the space between the outer casing and the rock formation (Figure 1).

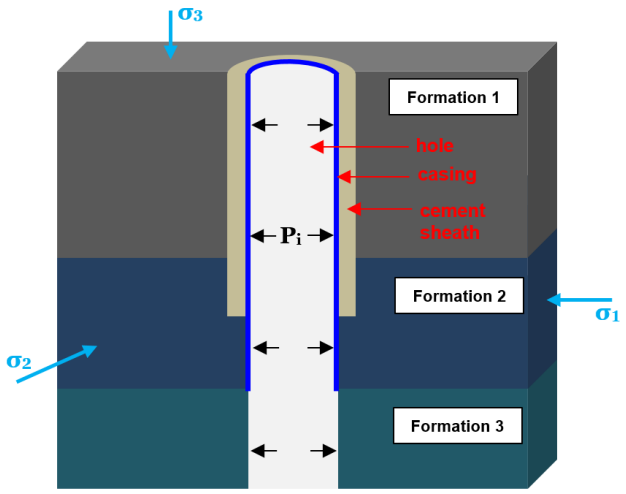

Figure 1. Well architecture, usually composed of hole, casing and cement sheath, after (Agofack and Cerasi, 2021).

The cement slurry hardens to become the cement sheath and play an important role as sealing barrier. However, during the above-mentioned subsurface activities, mechanical and thermal loadings are applied to casing and thus to the cement sheath and rock formation around. These can lead to cracks creation in the cement sheath which can propagate into the rock formation, and therefore constitute potential leakage paths (Bois et al., 2011; Petty et al., 2003). Additionally, the placement of the cement can also lead to the casing stand-off vis-à-vis to the cement sheath (De Andrade and Sangesland, 2016; De Andrade et al., 2014; Khodami et al., 2021). The casing stand-off is evaluated by the following formular (De Andrade and Sangesland, 2016; Mendez Restrepo et al., 2018; Weatherford, 2016):

$$\text{Stand-off}\,(\%) = \frac{C}{A-B} \times 100 \qquad (1)$$

where A and B are the radius of the hole and the outer radius of the casing, respectively, and C the smallest size between the casing and the hole wall, see Figure 2. A centered casing has stand-off of 100% while the extreme off centered one has a stand-off of 0%. In some regulations, the minimum stand-off of the casing should

be 70% (Queensland-Government, 2019). To achieve that, the casing centralizer are used during the running of the casing into the well (Juvkam-Wold and Wu, 1992; Lee et al., 1986; Weatherford, 2016). However, even with the used of centralizers, the stand-off of the casing still be less than 100%. The stand-off may affect the integrity of the well following mechanical and thermal loadings.

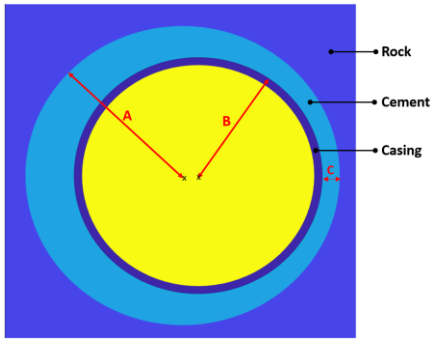

Figure 2. Casing stand-off, adapted from (Mendez Restrepo et al., 2018)

Existing experiments and simulations to investigate the cement sheath integrity are usually limited to the centralized casing case (Agofack and Cerasi, 2021; Anya et al., 2020; Gheibi et al., 2021; Gheibi et al., 2019; Goodwin and Crook, 1992; Skorpa et al., 2019; Skorpa et al., 2018; Vrålstad et al., 2021; Vrålstad et al., 2019). Only few studies have been dedicated to the effect of casing stand-off.

De Andrade et al. (2014) investigated the effect of casing centralization on cement sheath integrity submitted to thermal loading. 100% and 50% casing stand-off cases were experimentally studied. The rock and the casing were mounted into a pressure cell and the cement slurry was pumped to fill the annulus space while achieving the desired stand-off value. After cement curing for 5 days at 66°C and atmospheric pressure, the system was kept at room condition for two weeks before submitting to thermal cycles. The inner casing was then subjected to temperature variation with 100°C amplitude, while recording debonding and cracks with Acoustic Emission. Their results showed that the thermal cycling resistance of the cement sheath decrease when decreasing the stand-off. The propagation of the crack was higher in the 50% stand-off that in the centralized casing. By means of numerical simulation with finite elements method, De Andrade and Sangesland (2016) investigated the failure mechanisms of the cement sheath. The studied parameters included the cement's and formation's Young modulus, the in-situ cement hydrostatic stress as well as the casing stand-off, and poor casing placement with initial defects in cement sheath such debonding. The failure criterium in the cement sheath was defined as the ratio between representative stresses along cement sheath and the maximum allowable working stresses. According to the authors, the Young's modulus plays the major role in cement sheath failure while the casing stand-off has only minor effect. More recently, Khodami et al. (2021) performed some 3D simulations with Abaqus to study the effect casing stand-off on cement integrity under anisotropic in-situ stress similar to well's conditions. They found that under given condition of casing pressure and in-situ stresses, the plastic strain in the cement sheath increases with the decreases of casing stand-off, especially for stand-off values lower than 20%. The high plastic strain appears at the areas of shortest thickness of cement sheath, which also correspond to the area where most elements yielded. The authors therefore concluded that to prevent cement sheath going into plastic deformation, the minimum casing stand-off should be 20%, and that shortest thickness of the cement sheath should not be around the minimum horizontal stress. However, the previous studies do not give a conclusive answer regarding the effect of casing stand-off on cracks creation and propagation in the cement sheath after casing pressure loading. We therefore propose to investigate such effects in paper by means of numerical simulation. A modified discrete elements method is used. Applied boundary stresses are chosen to be representative of the in-situ stress. Both isotropic and anisotropic stress conditions are considered.

In the following sections, a description of the numerical code is given. The effect of the chosen numerical method on stress distribution is also highlighted. The description of the grid together with the used materials, and the calibration of the model with laboratory experiments are given in section § 3. The simulation results and discussion will then be given is section §4, and the paper will end with some conclusions.

2. NUMERICAL DESCRIPTION

For the numerical simulation, we have used a modified discrete element method (MDEM) code. The code is coupled with the open-source source MATLAB Reservoir Simulation Toolbox (MRST) and can simulate pore pressure changes, stress and displacement distribution as well as crack creation and propagation around the wellbore (Alassi, 2008; Alassi and Holt, 2012). It has been used in various wellbore integrity related investigations due to casing pressure changes, including among others the effect of cement hydration degree (Gheibi et al., 2019) and that of cement formation rock stiffness (Agofack and Cerasi, 2021). The boundary conditions are given in cartesian coordinates. The code is coupled with the open- code for fluid flow. This coupling makes it possible to simulate the fracture propagation and the fluid flow into it.

2.1. Stress and failure estimation near wellbore

The analytical derivation of stress distribution in a hollow cylinder and around the borehole can be found in different investigation (Agofack and Cerasi, 2021; Fjaer et al., 2008). The radial stress (σ_r) and tangential stress (σ_θ) for the hollow cylinder are given as:

$$\sigma_r = \frac{b^2 P_o - a^2 P_i}{b^2 - a^2} + \frac{a^2 b^2 (P_i - P_o)}{(b^2 - a^2) r^2} \quad (2)$$

$$\sigma_\theta = \frac{b^2 P_o - a^2 P_i}{b^2 - a^2} - \frac{a^2 b^2 (P_i - P_o)}{(b^2 - a^2) r^2} \quad (3)$$

and their expressions around a borehole with far-field anisotropic horizontal stresses (σ_1^∞ and σ_2^∞) are given by:

$$\sigma_r = \frac{\sigma_1^\infty + \sigma_2^\infty}{2}\left(1 - \frac{a^2}{r^2}\right) + \frac{\sigma_1^\infty - \sigma_2^\infty}{2}\left(1 - \frac{4a^2}{r^2} + \frac{3a^4}{r^4}\right)\cos 2\theta + P_i \frac{a^2}{r^2} \quad (4)$$

$$\sigma_\theta = \frac{\sigma_1^\infty + \sigma_2^\infty}{2}\left(1 + \frac{a^2}{r^2}\right) - \frac{\sigma_1^\infty - \sigma_2^\infty}{2}\left(1 - \frac{3a^4}{r^4}\right)\cos 2\theta - P_i \frac{a^2}{r^2} \quad (5)$$

According to equations (2) and (3), the stress distribution in hollow cylinder are independent of the angle θ. The same stress distribution, independent of θ is derived for concentric hollow cylinders, like presented in Figure 3, (Agofack and Cerasi, 2021). For a borehole with far-field isotropic stress ($\sigma_1^\infty = \sigma_2^\infty$), the terms related to $\cos 2\theta$ in equations (4) and (5) disappear, and the stress distribution become independent of the angle θ.

Table 1. Materials properties for analytical computation

Elastic properties	**Casing**	**Cement**	**Rock**
Young modulus [GPa]	210	10.4	24.68
Poisson ratio [-]	0.2	0.15	0.3
Radii [m]			
a	***a₁***	***a₂***	***b*** (rock half-size)
0.02815	0.03015	0.0381	0.2

For the numerical calculation using MDEM this becomes more complicated. MDEM calculates the forces on the vertex corners (nodes) of a triangular element grid. To calculate failure, the stress is estimated in each triangular element using the forces at the nodes. This estimation is not trivial and will produce an oscillatory stress pattern close to the hole caused by the variation in distance from the hole of the nodes and the rapid radial change in stress as shown in Figure 4. An average technique (Patch recovery) is used to smooth the stress field. However, the stress field in the elements with one node on the hole wall will still have a variation caused by the position of the off-wall node(s), see example in Figure 6. Although the variation is relatively small compared to the stress level, it will give a preferred direction of the initial crack to open and affect the stress level at which the first crack opens.

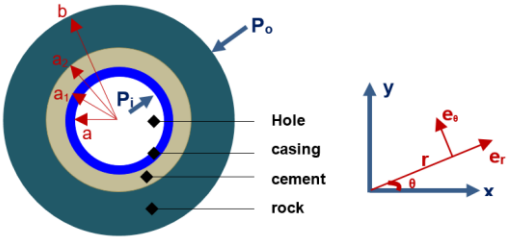

Figure 3. Concentric hollow cylinders with outer boundary conditions in polar coordinates (Agofack and Cerasi, 2021).

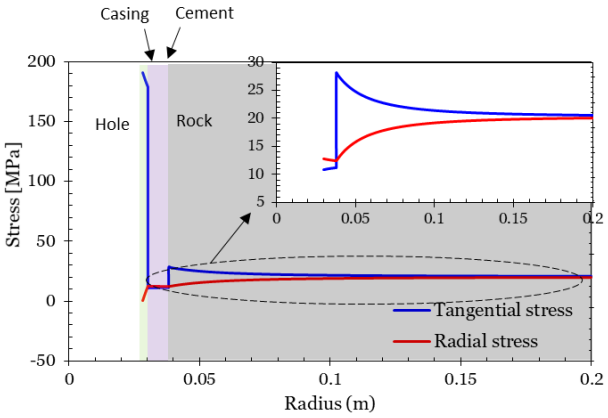

Figure 4. Computed variation of the tangential and radial stresses versus the radius from hole to the rock under an outer pressure of 20 MPa and a casing pressure of 1 MPa.

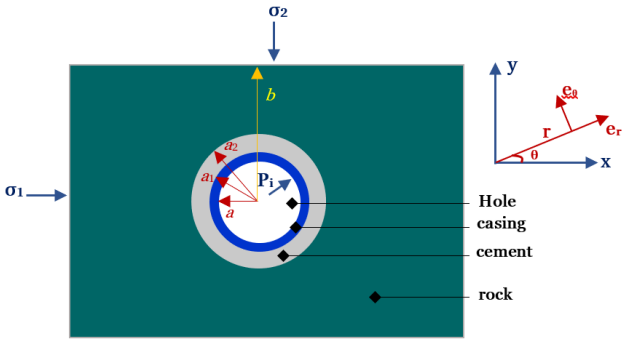

Figure 5. Concentric hollow cylinders in a field with outer boundary conditions in cartesian coordinates.

To experimentally investigate the fracture propagation due to casing pressure in oil/gas or CO_2 injection wells, the configuration of Figure 3 should be considered. It is composed of 3 concentric hollow cylinders, which are casing, cement, and rock. The inner pressure P_i corresponds to the casing pressure, while the outer pressure P_o corresponds to the confining pressure related to the in-situ stress. Its analytical solution for

displacement, strain and stress distributions versus the radius as well as the angle θ have been derived and published in previous investigation (Agofack and Cerasi, 2021). For the parameters given in Table 1, the computed distribution of the radial and tangential stresses is given in Figure 4. One can observe the discontinuity of the tangential stress at material interfaces, while the radial stress is continuous. When the concentric hollow cylinders are in a field with boundary in-situ stress given in cartesian coordinates (Figure 5), there is no obvious analytical solution of stress, strain, and displacement distribution around the wellbore, even for isotropic in-situ stress $(\sigma_1 = \sigma_2)$. Such distributions can be estimated by means of numerical codes (like MDEM).

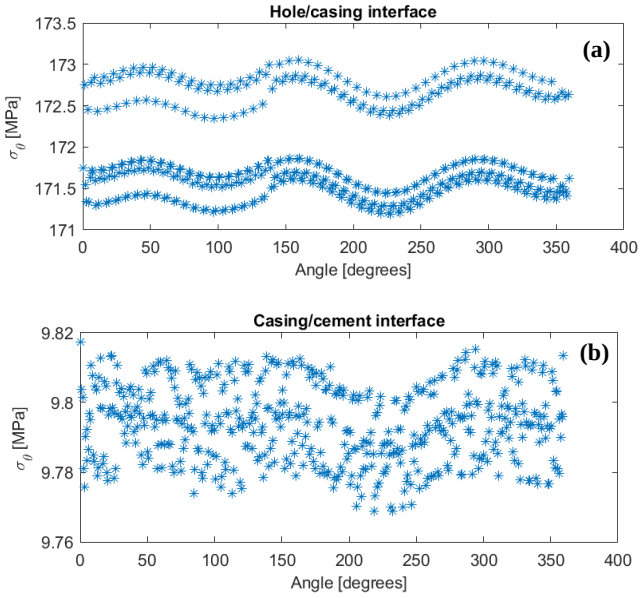

Figure 6. Numerical calculation of tangential stress distribution within casing (close to hole/casing interface) and at casing/cement interface versus angle θ for isotropic stress boundary stress of 20 MPa under a casing pressure of 0.2 MPa. For the first graph (Hole/casing interface), the top and bottom parts correspond to 0.15 mm and 0.30 mm within the casing, respectively.

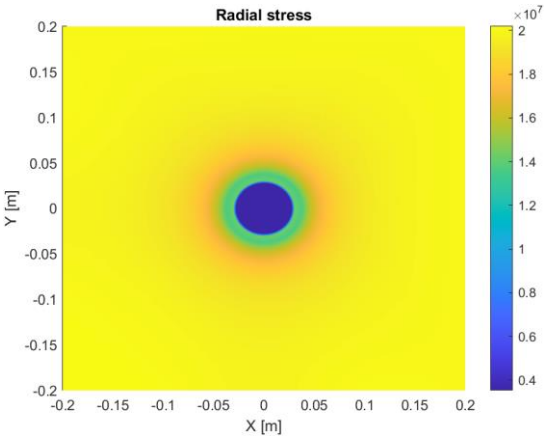

Figure 7. Numerical calculation of radial stress distribution within the casing versus angle θ when isotropic stress far-field stress of 20 MPa is applied, and the casing pressure is 0.2 MPa.

According to equations (4) and (5), the stress distribution around the well (in the casing, cement and the rock nearby) is expected to be independent of the angle θ, under isotropic in-situ stress. However, the numerical simulations showed that even with a well as small as 6 cm diameter in a field of 40 m size (b/a =1333, see Figure 5), the stress distribution around the borehole is stress affected by the numerical method used as previously discussed. . For the domain size used in the following simulations (b/a =7), the tangential stress at 0.15 mm and 0.30 mm within the casing is given in Figure 6 as function of the angle θ, and the radial stress for the entire grid is given in Figure 7. The tangential stress, which is responsible for cracks around the well (when it becomes negative, i.e., tensile) displays a kind of sinusoidal variation with θ, with its minimal values showing the places where the cracks are expected to be first created.

3. GRID, DIFFERENT MATERIAL AND MODEL CALIBRATION.

The grid in these simulations was built using the SALOME pre-and post-processing software. The grid consists of 6 different domains: hole, casing, interface casing/cement, cement, rock, and outer region (see Figure 8). The boundary conditions in terms stresses are applied at the outer boundary of the outer region. The variation of the casing pressure is achieved by injecting (or removing) fluid into (or from) the hole. The size of the outer region is 0.4m, 7 times larger than that of the hole. The total number of elements in the grid is around 40 000 and a simulation is usually completed in 7 days. The size of the outer region could be increased to reduce the boundary effect on cracks initiation and propagation. However, even when increasing its size to 100 times larger than that of the hole, it only lightly affects crack initiation and propagation, while the computing time drastically increases up to 20 days. The grid model, as presented in Figure 8, is similar for the different casing stand-off values investigated here. The mechanical properties used in the simulations were evaluated by laboratory experiments.

3.1. Materials used

The effect of casing stand-off was analyzed for two different rock formations: the Crab Orchard sandstone and the Draupne Shale. The choice of Draupne shale was motivated by its capacity to play as a caprock barrier for CO_2 storage in the North Sea, and the availability of its hydro-mechanical properties (Agofack et al., 2019; Skurtveit et al., 2015a; Skurtveit et al., 2015b; Smith et al., 2019); that of Crab Orchard was to highlight the effect of strength and stiffness contrast on crack propagation. The Portland G cement with slurry density of 1.90 g/cm^3 was used. The properties of different materials are given in Table 2. The outer region has the same properties as the rock, except the fact that it could be prevented from

failure by being assigned an extremely high tensile strength. The casing and hole regions are also prevented from failure. There is no fluid flow across the casing due to its extremely low permeability. Isotropic and anisotropic boundary effective stress were applied at the outer boundary of the outer region. The effect of casing stand-off was analyzed by applying similar boundary stress.

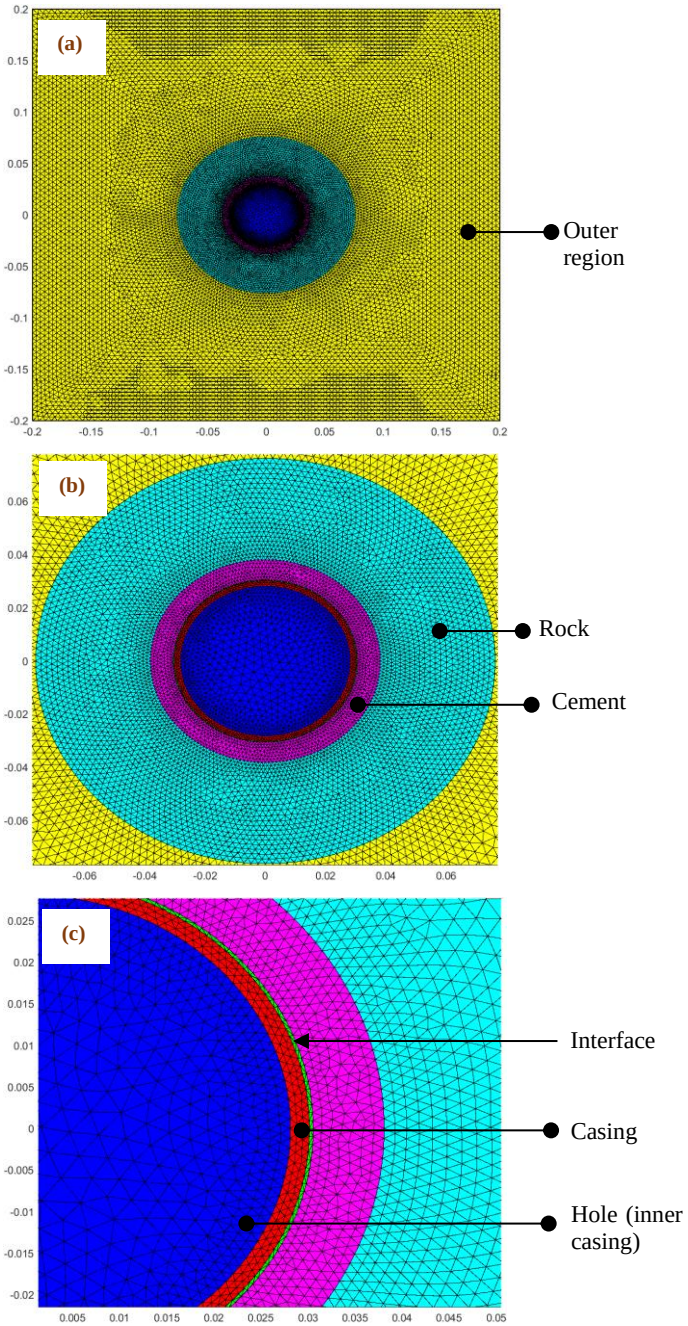

Figure 8. Mesh built with the SALOME software, centralized casing case (stand-off = 100%). (b) is a zoom from (a) and (c) a zoom from (b).

3.2. Calibration of parameters

The experimental results used for calibration were both performed under high and low confining pressure. The calibration for high confining pressure experimental (Taghipour et al., 2022), was successfully performed in a previous investigation for centralized casing (Agofack and Cerasi, 2021) and is presented Figure 9.

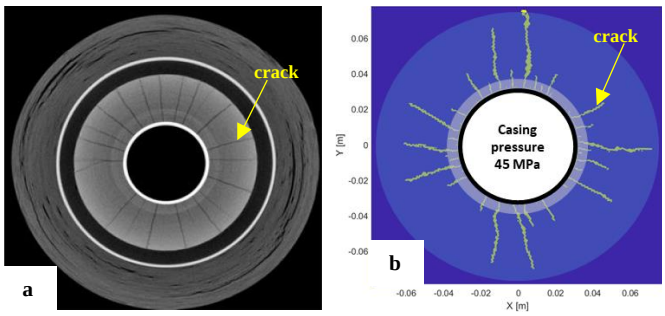

Figure 9. CT scans of casing experiment with Portland cement G and Castlegate sandstone under casing pressure of 45 MPa. (a) experiment under 8.5 MPa of confining pressure, (b) simulation with 7.5 MPa of isotropic boundary stress (Agofack and Cerasi, 2021).

For low confining experiments, results are presented in Figure 11 and Figure 12, and compared with the simulation for different rock and cement system. The experimental procedure is described in (Skorpa et al., 2019; Skorpa et al., 2018) and is briefly summarized here. After pumping the cement into the annular space between the casing the rock, it was hydrated at 66°C under 1 bar for 7 days. After this curing time, the confining pressure was kept at 1 bar, and the temperature brought to the ambient. The casing pressure was then rapidly increased to a given value in few seconds, and the setup (with the sample) was CT scanned to check if the applied casing pressure induced crack in the cement or rock. The pressure was released, and again rapidly increased to a value higher than the previous one, and another CT scan was made. The process was repeated until the end of the experiment (Figure 10).

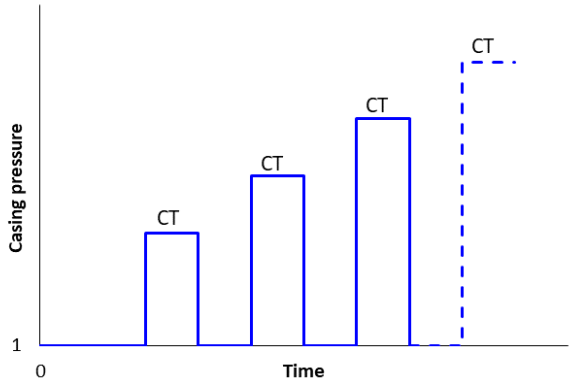

Figure 10. Procedure for pressure cycling experiments

The initial crack in the experiment appears under higher casing pressure than in the simulation. In the test with Castlegate sandstone (Figure 11), a full crack was built under a casing pressure of 230 bars while for the simulation a casing pressure 110 bars was sufficient to develop a full crack.

Table 2. Parameters of the different materials used in this simulation.

Material	Hole (inner casing)	Casing	Interface Casing/cement	Cement	Rock*		Outer Region*
					Crab Orchard	Draupne Shale	
Size: OD (mm)**	**56.3**	**60.3**	**61.1**	**76.2**	**152.4**		**400**
Young modulus [GPa]	0.28	210	2	10.0	**24.68**	**4.5**	
Poisson ratio [-]	0.48	0.30	0.15	0.15	0.3	0.28	
Porosity [-]	0.95	0.02	0.40	0.37	0.09	0.12	
Permability [m^2]	1×10^{-5}	1×10^{-23}	1×10^{-16}	1×10^{-16}	2×10^{-16}	3.2×10^{-22}	
Tensile strength σ_t [MPa]	10^{20}	10^{20}	1.5	6	12	2	

*The rock and outer region have similar properties ** OD stands for Outer Diameter.

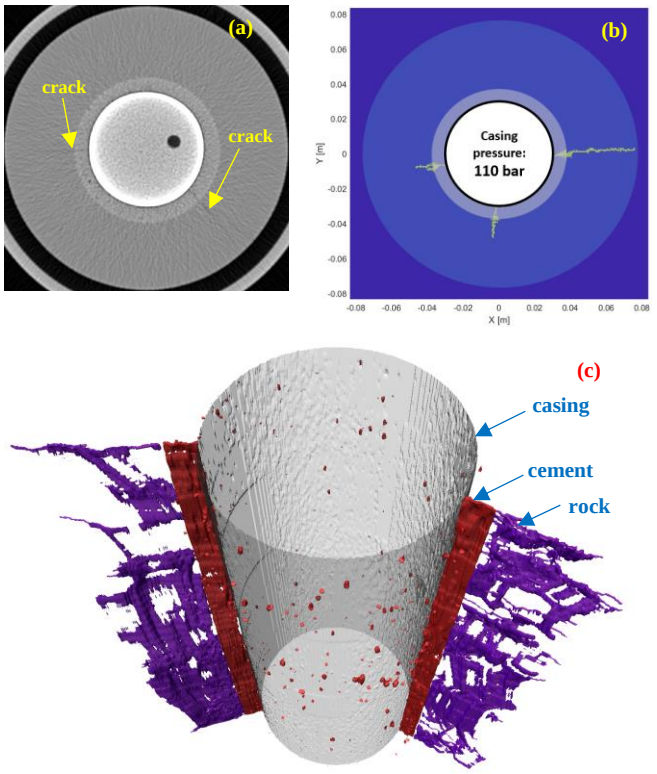

Figure 11. CT scans of casing experiment with Portland cement G and Castlegate sandstone under a confining pressure of 1 bar and casing pressure of 230 bars. (a) and (c) are from experiment, (b) simulation result under 1 bar of isotropic boundary stress.

For experiment with Crab Orchard sandstone, at the casing pressure of 260 bar, a full crack appears in the experiment while in the simulation two half-length cracks were observed. A plausible explanation between these differences is related loading rate of the casing pressure. In the experiment, the pressure change is almost instantaneous (Figure 10) while in numerical simulations and due to the convergence problem, the speed can be as low as 1bar/hour. Overall, the simulation reproduced well the experiments performed under different confining pressures and with different rock materials.

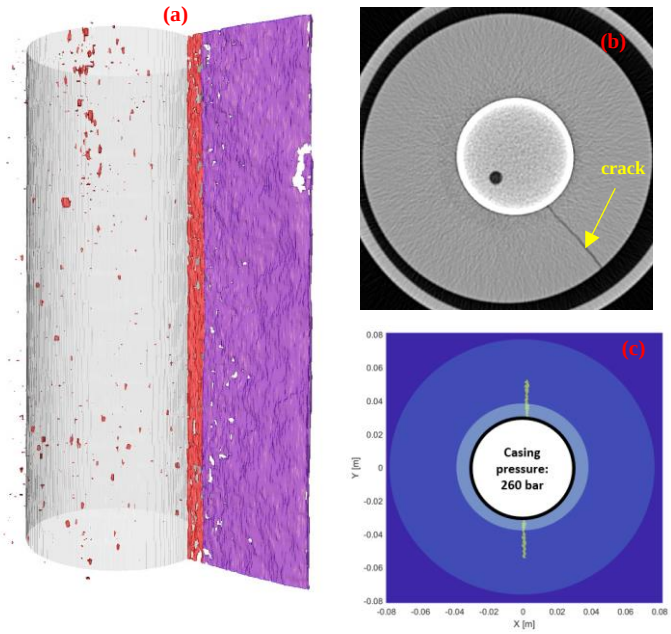

Figure 12. CT scans of casing experiment with Portland cement G and Crab Orchard sandstone under a confining pressure of 1 bar and casing pressure of 260 bars. (a) and (b) are from experiment, (c) simulation result under 1 bar of isotropic boundary stress.

4. RESULTS

Crab Orchard sandstone

A 100% and 50% stand-off cases are considered for this material. The tangential stress distribution around the hole/casing interface and casing/cement interface for 100% is like the plots of Figure 6 and Figure 7, respectively. For the 50% stand-off case, the tangential stress at the different interfaces is given in Figure 13 at casing pressures of 0.2 MPa and 53MPa. at the casing/cement interface, its variation with the angle θ is concave parabolic variation with minimal values at $\theta = 0°$ (and/or 360°). The form of the distribution is not affected by the casing pressure (Figure 13 b,d). However, around the hole/casing interface, the form of stress distribution is significantly affected by the casing pressure. Under low

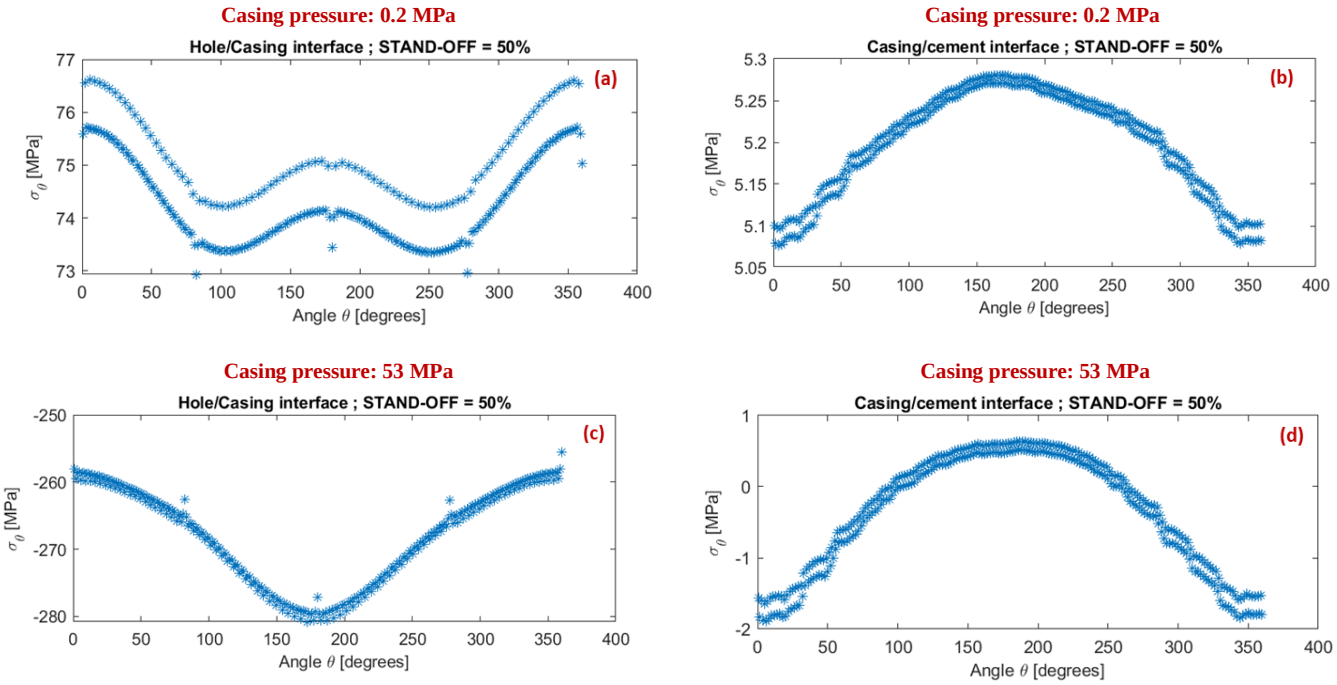

Figure 13. Tangential stress at the near the hole/casing interface (a, c) and at casing/cement interface (b, d) for isotropic boundary stress of 10 MPa and a casing pressure of 0.2 MPa (a, b), and 53 MPa (c,d), for casing stand-off of 50%.

casing pressure, it displays two minimum values at $\theta = 90°$ and $\theta = 270°$, while under the crack onset casing pressure, it shows a minimum value at $\theta = 180°$ (Figure 13 a,c). The region where the crack first started seems to be determined the tangential stress at both hole/casing and casing/cement interfaces. The results of crack propagation are presented in Figure 14 for three different casing pressure 70 MPa, 100 MPa and 120 MPa. The casing pressure required to start the crack is 52 MPa and 53 MPa for 100% and 50% stand-off, respectively. At a given casing pressure, the number of cracks as well as the size of the major ones are slightly the same for the two stand-off cases. As mentioned in section §2, the main direction of crack propagation are long the x and y-axis where four major cracks are developed. Under a casing pressure up to 120 MPa, only few cracks have propagated some 30 mm into the rock while most of them remain in the cement sheath.

The effect of anisotropic boundary stress was also investigated. The two different casing stand-offs of Figure 14 were simulated under anisotropic stresses while keeping parameters constants. Three cases were simulated. In cases 1 and 2, the effective boundary of 10 MPa and 15 MPa were applied along x- and y-axis, respectively. In case 3, the direction of maximum boundary stress was switched. The results are presented in Figure 15 for different casing pressures (70, 100 and 120 MPa). The casing pressure required to create cracks in the cement sheath was 53 MPa, 50 MPa and 51 MPa for cases 1, 2 and 3, respectively. The 50% stand-off seems to have slightly decreased cement sheath failure pressure. Regardless the casing stand-off, the cracks preferentially propagate along the direction of the maximum horizontal stress, which represent the direction of minimum tangential stress. Similar observations have been made on extended leak-off tests (Lavrov et al., 2015). At a given casing pressure, the effect of casing stand-off on crack's size seems to be minor, as also concluded by De Andrade and Sangesland (2016).

Draupne Shale

More casing stand-off scenarios were considered in this case including 0, 25, 50, 75 and 100% stand-off. The 100% corresponds to the centered casing while the 0% correspond to case where the casing is in contact with the rock formation and thus exposed to corrosion. The effective boundary stress was kept at 10 MPa. The results are summarized in Figure 16 for three different casing pressures. The three columns correspond to the plotted casing pressures while the rows represent different casing stand-offs with their written inside the hole. For example, the Figure 16f represents the crack distribution in cement sheath and rock for 75% casing stand-off, at a casing pressure of 100 MPa and under the effective boundary stress of 10 MPa. For a given stand-off case, the obvious results show that the cracks increased with the casing pressure. When the casing pressure is fixed, the number of cracks is inversely proportional to the stand-off values: more cracks are created under lower stand-off values. The results further show that the cracks are almost only within the cement sheath. When comparing for example Figure 14d and Figure 16i which correspond to the casing stand-off of 50% at the same casing pressure, but for different rocks, it appears that the softer the rock the higher the

number of cracks is and the shorter their propagation into the rock formation. In other words, for the soft rock case (Draupne Shale, Figure 16i) more cracks are created but are all with the cement sheath, while for stiffer rock (Crab Orchard, Figure 14d) fewer cracks are created but have propagated deeper into the rock. The results is in line with our previous founding on role placed by the rock stiffness on cracks propagation behind the casing (Agofack and Cerasi, 2021). It was also observed that the casing pressure required to initiate crack decreases with the decrease of the stand-off value. It was 43 MPa for the 100% stand-off case and reduced to 28 MPa for 0% stand-off.

The effect of the boundary stress was also investigated and are presented in Figure 17. Three different isotropic boundary effective stresses were considered: 10, 15 and 25 MPa, and the centered casing case was used. Draupne Shale was the rock material. The obvious results show that the higher the boundary stress the higher the required casing pressure to initiate cracks is. At a given casing pressure, the number of cracks as well as their sizes decrease with in the increase of the boundary stresses. At a casing pressure as high as 120 MPa, most cracks were still limited with the cement sheath regardless the boundary stress.

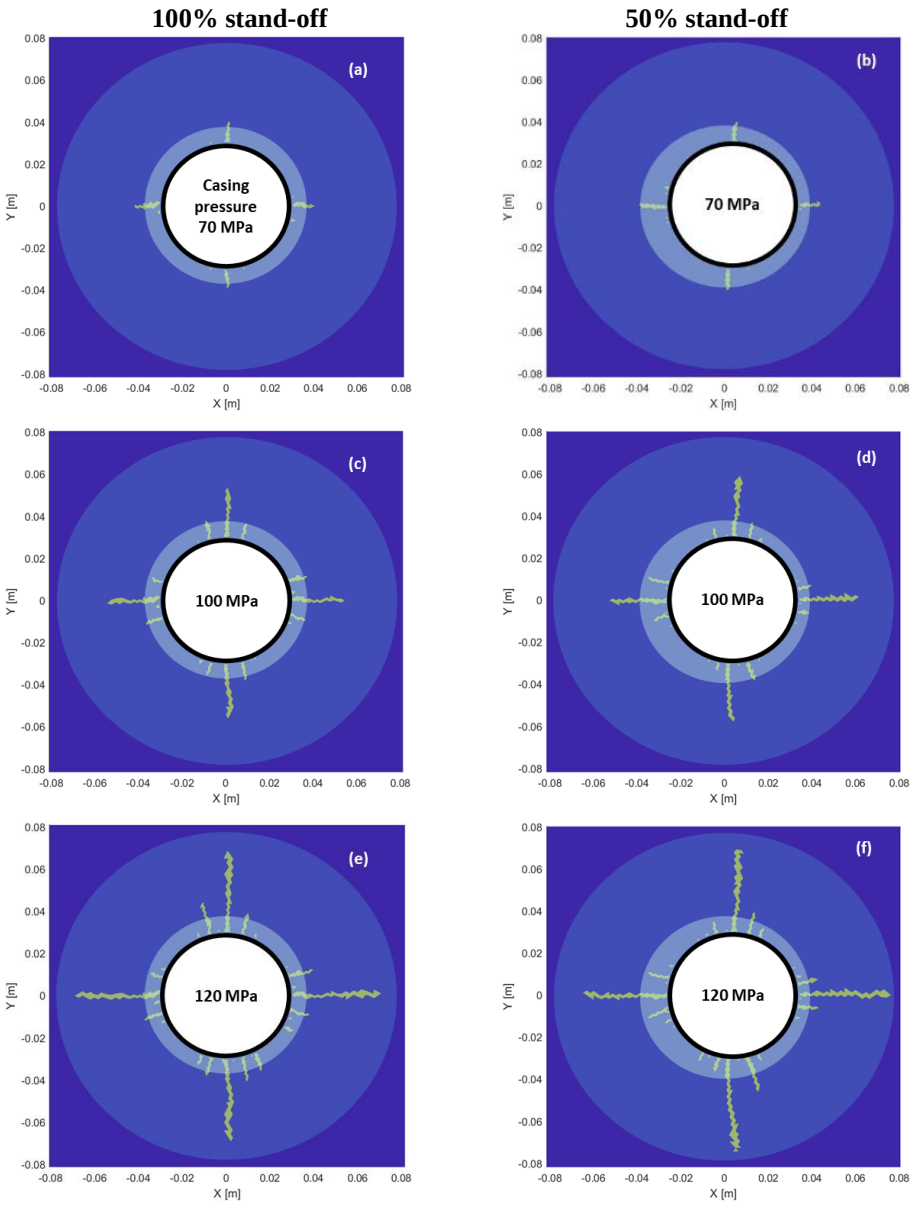

Figure 14. Portland cement G and Crab Orchard sandstone under a boundary stress of 10 MPa and at different casing pressures.

5. CONCLUSIONS

A numerical method has been used in this paper investigate the effect of casing stand-off on cracks initiation and propagation around the borehole. The properties of Portland cement G were used for the cement sheath, while two different materials were considered for the rock formations. The Crab Orchard sandstone with high stiffness and the Draupne Shale as potential caprock material were used. The casing stand-off investigated were 0% (a casing touching the rock), 25%, 50%, 75% and 100% (a centered casing). After the calibration of the model laboratory tests performed under both low and high confining pressure, an isotropic boundary stress of 10 MPa for all the simulated cases. The results showed that for a given casing pressure, the number of cracks created as well as their size is less affected by the casing stand-off between 50% and 100%. A noticeable discrepancy appears when comparing a centered casing case and the 0% stand-off. The required casing pressure to initiate crack is also high in these two extremes cases: 28 MPa and 43 MPa for 0% and 100% stand-off, respectively. As previously highlighted (Agofack and Cerasi, 2021), the crack creation and propagation is also a function of the rock stiffness. For the Crab Orchard sandstone case, a casing pressure 52 MPa was needed to start a crack in the cement for the centered casing case. The effect boundary stress was also analyzed, and the obvious results show that the higher the boundary stress the fewer the created cracks at a given casing pressure. At a casing pressure as high as 120 MPa, most cracks were still limited with the cement sheath in the soft rock case. Such high casing pressures can happen in the field only in accidental situation.

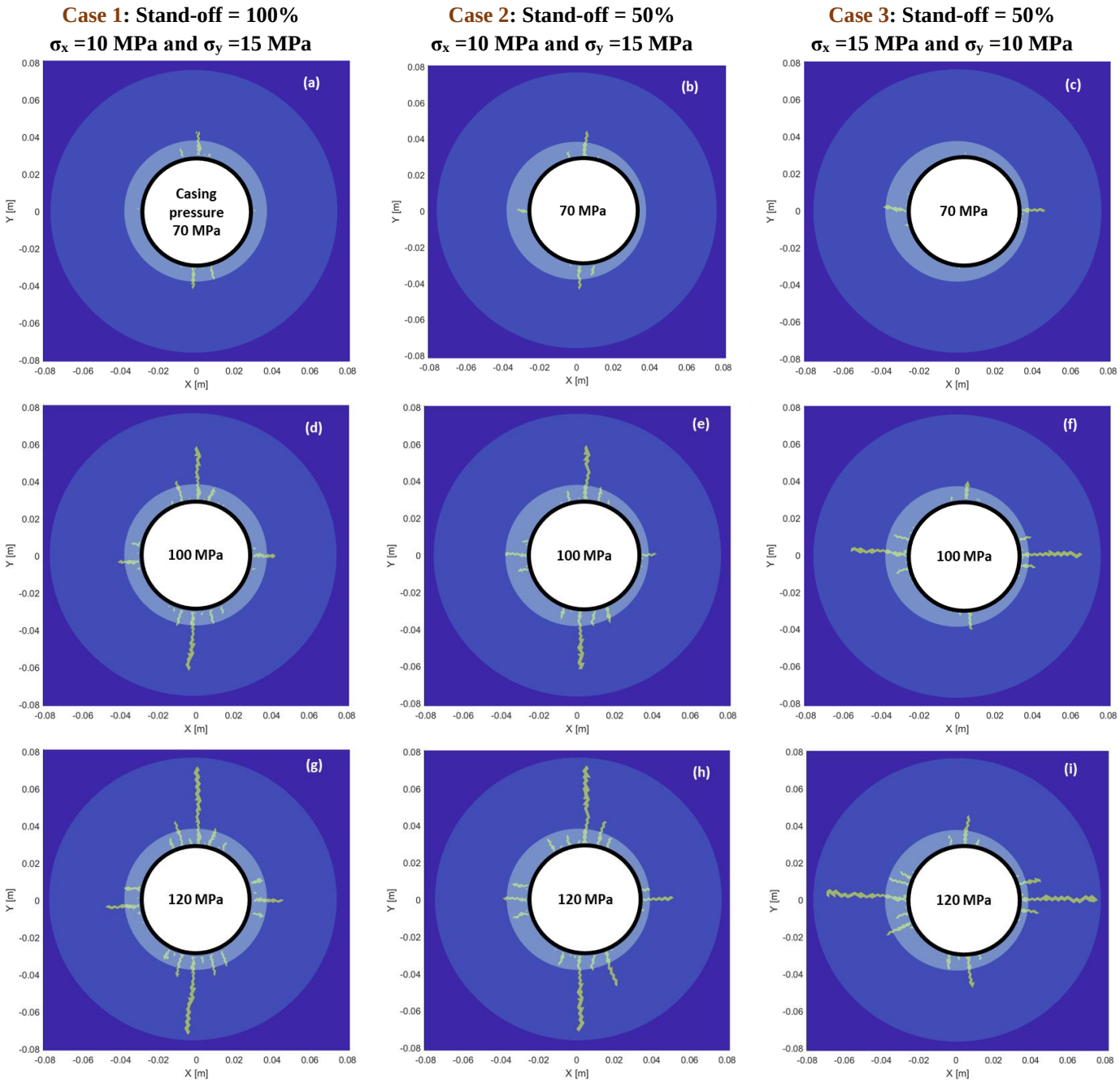

Figure 15. Effect of boundary stress anisotropy on cracks propagation for 100% and 50% casing stand-off at different casing pressures. Cases 1 and 2 analyse the effect of casing stand-off under similar anisotropic boundary stresses: 10 MPa and 15 MPa in the x- and y- direction, respectively. Cases 2 and 3 analyse the direction of anisotropic for similar casing stand-off.

6. AKNOWLEDGEMENTS

This publication has been produced with support from the REX-CO_2 (re-using existing wells) project which has received funding from ADEME (FR), RVO (NL), Gassnova (NO), UEFISCDI (RO), BEIS (UK), and DOE (USA), and is cofounded by the European Commission under the Horizon 2020 program ACT, Project No. 299681.

7. REFERENCES

Agofack N., Cerasi P. (2021) Numerical simulation of fractures propagation around the wellbore: Effect of the surrounding rock's stiffness, in: ARMA (Ed.), 55th US Rock Mechanics/Geomechanics Symposium, Houston, Texas, USA.

Agofack N., Cerasi P., Stroisz A., Rørheim S. (2019) Sorption of CO2 and integrity of a caprock shale, 53rd US Rock Mechanics/Geomechanics Symposium, ARMA.

Alassi H.T. (2008) Modeling reservoir geomechanics using discrete element method: Application to reservoir

monitoring, Norwegian University of Science and Technology.

Alassi H.T., Holt R. (2012) Relating discrete element method parameters to rock properties using classical and micropolar elasticity theories. International Journal for Numerical and Analytical Methods in Geomechanics 36:1350-1367. DOI: 10.1002/nag.1056.

Anya A., Emadi H., Watson M. (2020) Computed Tomography Study of Annular Cement Mechanical Response Under Cyclic Hydraulic Stress, Proceedings of the 8th Unconventional Resources Technology Conference.

Bois A.-P., Garnier A., Saint-Marc J., Aimard N. (2011) How To Prevent Loss of Zonal Isolation Through a Comprehensive Analysis of Microannulus Formation, in: SPE (Ed.), SPE Annual Technical Conference and Exhibition, New Orleans, Louisiana.

De Andrade J., Sangesland S. (2016) Cement Sheath Failure Mechanisms: Numerical Estimates to Design for Long-Term Well Integrity. Journal of Petroleum Science and Engineering 147:682-698. DOI: 10.1016/j.petrol.2016.08.032.

De Andrade J., Torsaeter M., Todorovic J., Opedal N., Stroisz A., Vrålstad T. (2014) Influence of Casing Centralization on Cement Sheath Integrity During Thermal Cycling, in: SPE (Ed.), 2014 IADC/SPE Drilling Conference and Exhibition, IADC/SPE Fort Worth, Texas, USA. pp. 10.

Fjaer E., Holt R.M., Horsrud P., Raaen A.M., Risnes R. (2008) Petroleum related rock mechanics. 2nd ed.

Gheibi S., Agofack N., Sangesland S. (2021) Modified discrete element method (MDEM) as a numerical tool for cement sheath integrity in wells. Journal of Petroleum Science and Engineering 196. DOI: 10.1016/j.petrol.2020.107720.

Gheibi S., Sangesland S., Vrålstad T. (2019) NUMERICAL MODELING OF RADIAL FRACTURING OF CEMENT SHEATH CAUSED BY PRESSURE TESTS, Proceedings of the ASME 2019 38th International Conference on Ocean, Offshore and Arctic Engineering OMAE2019, ASME, Glasgow, Scotland.

Goodwin K.J., Crook R.J. (1992) Cement Sheath Stress Failure. SPE Drilling Engineering,:6.

Juvkam-Wold H.C., Wu J. (1992) Casing Deflection and Centralizer Spacing Calculations. Society of Petroleum Engineers:7.

Khodami E., Ramezanzadeh A., Sharifi A. (2021) The 3D simulation of the effect of casing standoff on cement integrity by considering the direction of horizontal stresses in one of the wells of Iranian oil fields. Journal of Petroleum Science and Engineering 206. DOI: 10.1016/j.petrol.2021.108980.

Lavrov A., Larsen I., Bauer A. (2015) Numerical Modelling of Extended Leak-Off Test with a Pre-Existing Fracture. Rock Mechanics and Rock Engineering 49:1359-1368. DOI: 10.1007/s00603-015-0807-x.

Lee H.K., Smith R.C., Tighe R.E. (1986) Optimal Spacing for Casing Centralizers. Society of Petroleum Engineers:122.

Mendez Restrepo M.F., Ichim A., Teodoriu C. (2018) The Effect of Wellbore Centralization in Geothermal Wells, 43rd Workshop on Geothermal Reservoir Engineering, Stanford University, Stanford, California. pp. 8.

Petty S., Gastineau J., Bour D.L., Ravi K. (2003) LIFE CYCLE MODELING OF WELLBORE CEMENT SYSTEMS USED FOR ENHANCED GEOTHERMAL SYSTEM DEVELOPMENT, Twenty-Eighth Workshop on Geothermal Reservoir Engineering, Stanford University, Stanford, California, USA. pp. 11.

Queensland-Government. (2019) Code of Practice For the construction and abandonment of petroleum wells and associated bores in Queensland Petroleum and Gas Inspectorate, in: M. a. E. Department of Natural Resources (Ed.), State of Queensland,. pp. 76.

Skorpa R., Werner B., Vrålstad T. (2019) Effect of Mud on Cement Sheath Integrity, SPE Norway One Day Seminar, Bergen, Norway.

Skorpa R., Øia T., Taghipour A., Vrålstad T. (2018) LABORATORY SET-UP FOR DETERMINATION OF CEMENT SHEATH INTEGRITY DURING PRESSURE CYCLING, ASME 2018 37th International Conference on Ocean, Offshore and Arctic Engineering, Madrid, Spain.

Skurtveit E., Choi J.C., Soldal M., Grande L., Maurer R., Horsrud P. (2015a) Mechanical Anisotropy Characterization of the Draupne Formation, North Sea, Fourth International Conference on Fault and Top Seals, Alméria, Spain.

Skurtveit E., Grande L., Ogebule O.Y., Gabrielsen R.H., Faleide J.I., Mondol N.H., Maurer R., Horsrud P. (2015b) Mechanical testing and sealing capacity of the Upper Jurassic Draupne Formation, North Sea, 49th US Rock Mechanics / Geomechanics Symposium, San Francisco, CA, USA. pp. 8.

Smith H., Bohloli B., Skurtveit E., Mondol N.H. (2019) Engineering Parameters of Draupne Shale-Fracture Characterization and Integration with Mechanical Data, Sixth EAGE Shale Workshop.

Taghipour A., Ghaderi A., Cerasi P., Gheibi S. (2022) Novel laboratory setup for realistic wellbore cement and formation integrity studies. Journal of Petroleum Science and Engineering 208:7.

Vrålstad T., Skorpa R., Opedal N., Todorovic J., Agofack N., Nguyen H.H. (2021) Cement Sheath Integrity during High Temperature Geothermal Well Operations, ASME 2021 40th International Conference on Ocean, Offshore and Arctic Engineering OMAE2021 ASME. pp. V010T11A033-1 - V010T11A033-8.

Vrålstad T., Skorpa R., Werner B. (2019) Experimental Studies on Cement Sheath Integrity During Pressure Cycling, in: SPE (Ed.), SPE/IADC International Drilling Conference and Exhibition, The Hague, The Netherlands.

Weatherford. (2016) Well construction Casing Accessories, cement integrity starts here, in: Weatherford (Ed.).

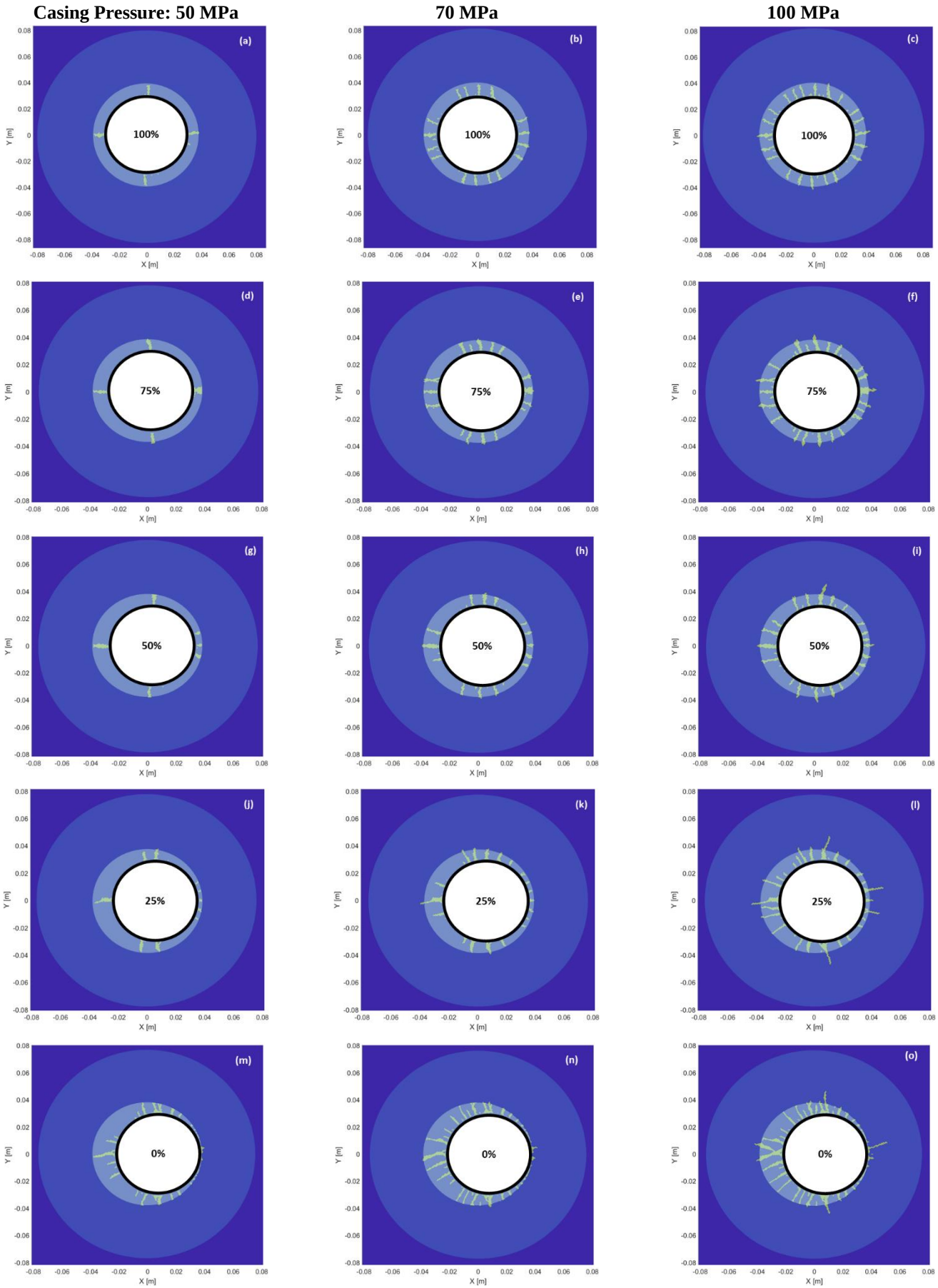

Figure 16. Effect of casing stand-off on cracks propagation in the cement sheath and rock for different casing pressures

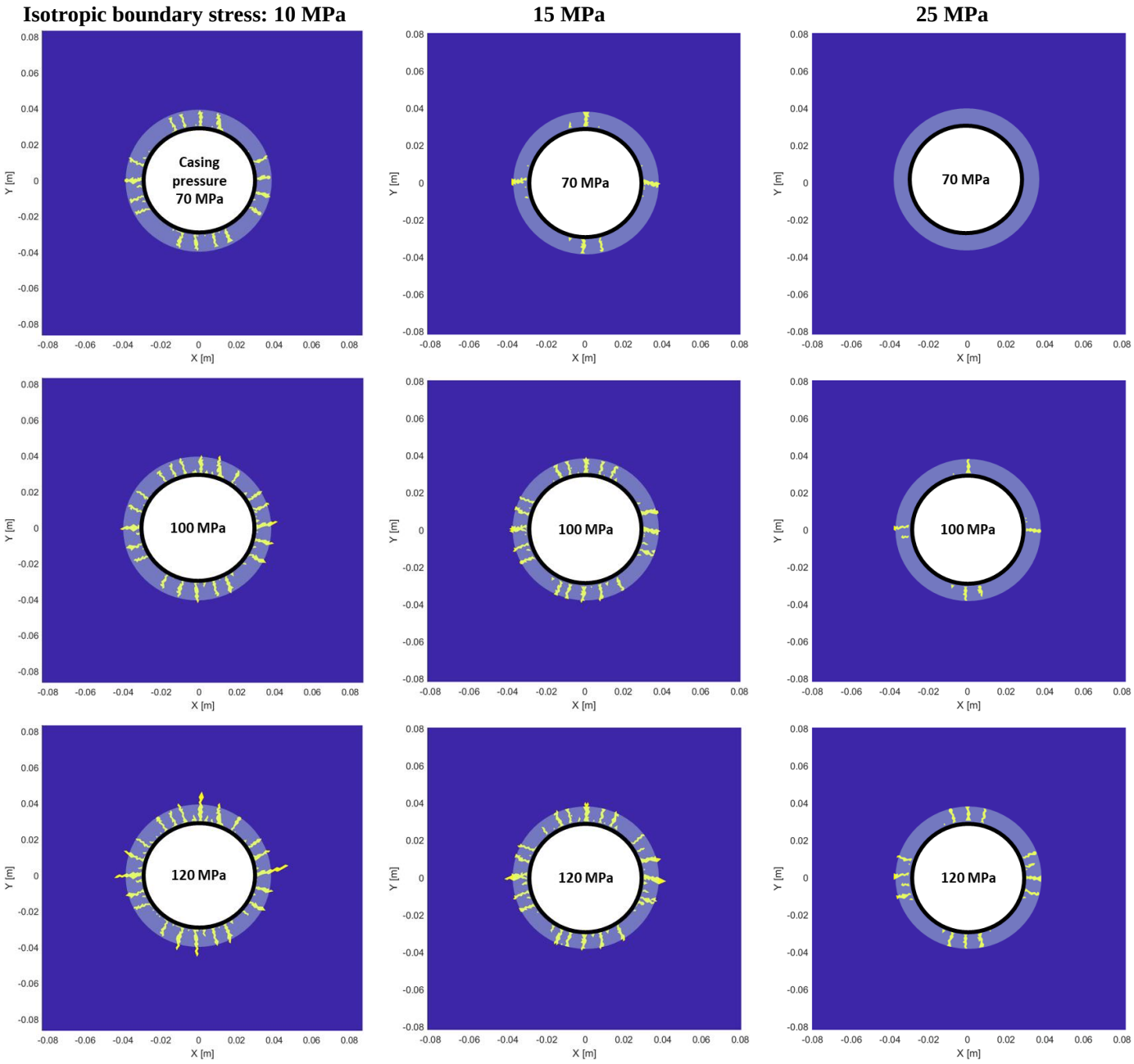

Figure 17. Effect of boundary stress on crack propagation for a 100% casing stand-off at different casing pressures. The casing pressure for crack creation is 43 MPa, 56 MPa and 85 MPa under isotropic effective boundary stress of 10 MPa, 15 MPa and 25 MPa, respectively.